Accepted Manuscript

Functional Materials Letters

Article Title:	MnO_2 nanowires-decorated carbon fiber cloth as electrodes for aqueous asymmetric supercapacitor
Author(s):	Congcong Hong, Xing Wang, Houlin Yu, Huaping Wu, Jianshan Wang, Aiping Liu
DOI:	10.1142/S1793604718500340
Received:	26 January 2018
Accepted:	15 March 2018
To be cited as:	Congcong Hong *et al.*, MnO_2 nanowires-decorated carbon fiber cloth as electrodes for aqueous asymmetric supercapacitor, *Functional Materials Letters*, doi: 10.1142/S1793604718500340
Link to final version:	https://doi.org/10.1142/S1793604718500340

World Scientific
www.worldscientific.com

Functional Materials Letters
Vol. 1, No. 1 (2018) 1–4

MnO_2 nanowires-decorated carbon fiber cloth as electrodes for aqueous asymmetric supercapacitor

Congcong Hong, [†] Xing Wang, [†] Houlin Yu, [†] Huaping Wu, [‡] Jianshan Wang, [‖] and Aiping Liu [*,†,§]
[†] *Center for Optoelectronics Materials and Devices, Zhejiang Sci-Tech University, Hangzhou 310018, China*
[‡] *Laboratory of E&M (Zhejiang University of Technology), Ministry of Education & Zhejiang Province, Hangzhou 310014, China*
[‖] *Tianjin Key Laboratory of Modern Engineering Mechanics, Department of Mechanics, Tianjin University, Tianjin 300072, China*
[§] *State Key Laboratory of Structural Analysis for Industrial Equipment, Dalian University of Technology, Dalian 116024, China*
[*] *liuaiping1979@gmail.com*

Received 26 January 2018[*]

MnO_2 nanowires (NWs) anchored on carbon fiber cloth were fabricated through a simple hydrothermal reaction and used as integrated electrodes for supercapacitor. The morphology-dependent electrochemical performance of MnO_2 NWs was confirmed, yielding good capacitance performance with a high specific capacitance of 3.88 F·cm^{-2} at a charge-discharge current density of 5 mA·cm^{-2} and excellent stability of 91.5% capacitance retention after 3000 cycles. Moreover, the composite electrodes were used to fabricate supercapacitors which showed a high specific capacitance of 194 mF·cm^{-2} at a charge-discharge current density of 2 mA·cm^{-2} and high energy density of 0.108 mWh·cm^{-2} at power density of 2 mW·cm^{-2}, foreboding its potential application for high-performance supercapacitor.

Keywords: MnO_2 nanowires, carbon fiber cloth, supercapacitor, energy density, power density.

With the gradual increase in the demand for energy and power in many fields such as portable electronic equipment, medical equipment and transportation, the supercapacitors have attracted worldwide attention due to the advantages of fast charge-discharge rate, high power density and long-term stability.[1-3] Compared to electric double layer capacitors that use carbon-based active materials,[4,5] pseudocapacitive electrode materials can provide higher specific capacitance and energy density.[6] Thereinto, manganese dioxide (MnO_2) is considered as a promising supercapacitor electrode material due to its low cost, environmental friendliness and high theoretical specific capacitance (1370 F/g).[4,7,8] Nevertheless, the poor electrical conductivity of MnO_2 damages its electrochemical activity. Up until now, extensive efforts have been made to design MnO_2-based electrode materials, aiming at improving the conductivity or promoting electrochemical performance.[9-15] However, many MnO_2-based electrodes are prepared by conventional slurry-coating technique, where the binder greatly reduces the conductivity of active material and hinders rapid electron transport.[4] Therefore, the direct growth of MnO_2 nanomaterials on conductive substrates with high specific surface area is an effective method to avoid binders or conductive additives use and enhance the electrical contacts between MnO_2 and conductive substrates for better Faraday's energy storage.

The morphology of active material greatly affects its performance, therefore it's important to study the relationship between them. Many morphology-controlled MnO_2 including nanorods, nanosheets, nanoparticles and so on have been reported in previous works. However, the investigation related to MnO_2 nanowires (NWs) with high specific surface is limited. In this work, we fabricated MnO_2 NWs on carbon fiber cloth (CFC/MnO_2) via the hydrothermal method. By changing the reaction time of hydrothermal synthesis, the morphology and electrochemical performance of CFC/MnO_2 composites were successfully adjusted. The morphology-dependent electrochemical performances of composites were confirmed by various electrochemical measurements. Additionally, the asymmetric supercapacitors were assembled by using the CFC/MnO_2 composites and

[*] Corresponding author.

activated carbon (AC) on CFC (CFC/AC) as positive electrode and negative electrode, respectively, and a high specific capacitance of 194 mF·cm^{-2} at a charge-discharge current density of 2 mA·cm^{-2} and a high energy density of 0.108 mWh·cm^{-2} at power density of 2 mWh·cm^{-2} were obtained. Our result is helpful for understanding the effect of reaction condition of MnO_2 on the tunable morphology and electrochemical performance of composites.

The CFC/MnO_2 was synthesized according to previous reported method.[4] Briefly, CFC pieces (40mm×10mm) were cleaned with acetone, ethanol and distilled water, and dried at 60℃ for 6h. Then the CFC was placed standing against the wall of a Teflon-lined autoclave with reaction solution of $KMnO_4$ (0.06 mol/L). In order to investigate the influence of reaction time to the morphology and performance of CFC/MnO_2 composites, the hydrothermal reaction happened at 140 ℃ for 1h, 3h, 6h, and 9h, respectively, followed by natural cooling to ambient temperature. After that, the CFC/MnO_2 composites were rinsed several times to remove the residuals, and dried at 60 ℃ in an oven overnight for use.

The crystalline structures of as-prepared materials were identified by a Bruker D8 Discover X-ray powder diffractometer (XRD, Cu Kα, λ=0.15418nm). The morphologies and microstructures were studied by using a field emission scanning electron microscopy (FESEM, Hitachi S-4800) and transmission electron microscopy (TEM, JEOL 2100, Japan). X-ray photoelectron spectroscopy (XPS) was carried out on a Kratos' Axis Ultra DLD (delay line detector) photoelectron spectrometer. The electrochemical performances of composites (1cm^2 in area) were evaluated by using a CHI 760E electrochemical workstation (CH Instruments, China) in a Na_2SO_4 solution (1 mol/L) by using a Pt foil as counter electrode and a saturated calomel electrode (SCE) as reference electrode. Cyclic voltammograms (CVs) were obtained at different scan rates in the potential range from 0V to 1.0V (vs. SCE). Galvanostatic charge/discharge (GCD) properties were measured at step increasing current densities of 5-20 mA·cm^{-2} from 0-1.0V. Electrochemical impedance spectra (EIS) were measured using a frequency range between 100 kHz and 0.01 Hz with 5-mV amplitude at open circuit potential. The area-specific capacitance (C) was calculated from CVs and GCD curves according to the equations $C_1 = (\int I_1 dV)/vs\Delta V$ and $C_2 = (I_2\Delta t)/s\Delta V$. Here, I_1 is the response current (mA), v is the scan rate (mV·s^{-1}), I_2 is the discharge current (mA), Δt is the discharge time (s), s is the area (cm^2) of active materials and ΔV is the potential range (V). Furthermore, the asymmetric supercapacitors (CFC/MnO_2//CFC/AC-ASC) were assembled by using the CFC/MnO_2 composites and CFC/AC[16] as positive electrode and negative electrode with a filter paper separator sandwiched in between (1 M Na_2SO_4 solution as electrolyte). The electrochemical performance of supercapacitor was evaluated using CR2032-type coin cells. The C of asymmetric supercapacitors was also calculated. In addition, the power density P (W·cm^{-2}) and energy density E (Wh·cm^{-2}) were calculated based on the equations $E = (1/2)C\Delta V^2$ and $P = E/t$, where ΔV (V) is the potential window, and t (s) is the discharge time.

Fig. 1 shows SEM images of CFC/MnO_2 composites prepared at different reaction periods. After hydrothermal reaction for 1h, the CFC substrate is completely covered with accumulated sphere-like MnO_2 nanoparticles (Fig.1a-b). When the time reaches 3h, the nanoparticles are transformed to MnO_2 NWs with a length of tens of micrometers and a diameter of 5-30nm (Fig.1c-d). Further increase the reaction time to 6h and 9h, the MnO_2 NWs evolve into MnO_2 nanorods with a length of several micrometers and a diameter of 10-60 nm (Fig.1e-h). The morphology of MnO_2 NWs is also observed by the TEM technology (Fig. 1i). The high-resolution TEM (HRTEM) image in Fig. 1(j) reveals well-resolved lattice fringes of about 0.24 nm, corresponding to the (211) plane of α-MnO_2.[17]

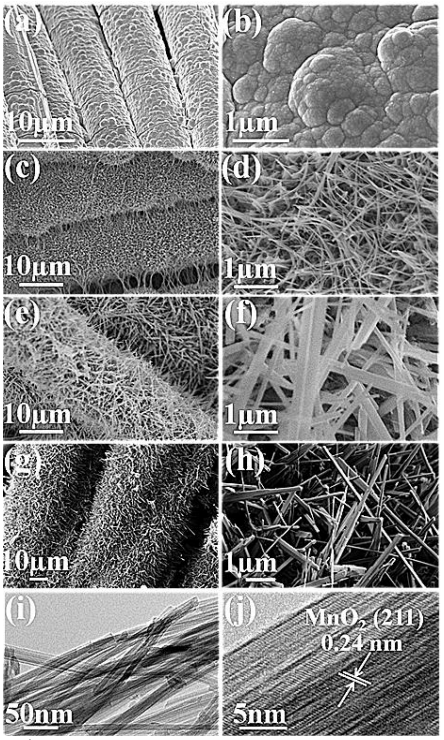

Fig. 1. Low- and high-magnification SEM images of CFC/MnO_2 composites obtained at 140℃ for different reaction times: (a-b) 1 h, (c-d) 3 h, (e-f) 6 h, (g-h) 9 h. (i) TEM and (j) HRTEM images of MnO_2 NWs obtained at the hydrothermal reaction for 3h.

Fig. 2(a) shows the XRD patterns of pure CFC and CFC/MnO_2 composites. The characteristic peaks of CFC are mainly located at about 2θ=25.5˚, 43.8˚ and 64.3˚. Compared with CFC, two characteristic peaks at around 2θ=37.2˚ and 66.0˚ appear in the CFC/MnO_2 spectrum, corresponding to (211) and (002) lattice planes of α-MnO_2 (JCPDS card No. 44-0141).[17,18] This is consistent with the TEM result in Fig. 1(j). Additionally, the peak related to CFC is obviously weakened after MnO_2 deposition because of the increased MnO_2 loading on CFC surface. Figs. 2(b-d) show XPS spectra of CFC/MnO_2. The full spectrum clearly shows the characteristic peaks of C, Mn and O elements (Fig. 2b). The high-resolution Mn 2p spectrum in Fig. 2(c) shows two distinct characteristic peaks, corresponding to Mn $2p_{3/2}$ (642.4eV) and Mn $2p_{1/2}$ (654.0eV), respectively. The distance between these two peaks is about 11.6eV, indicating that the Mn element exists mainly as +4 valent state.[19-21] Fig. 2(d) shows the O 1s spectrum with three fitting Gaussian peaks, corresponding to the O atoms in MnO_2 (Mn-O-Mn at 529.7 eV), hydroxyl group (Mn-O-H at 531.2 eV) and adsorbed water (H-O-H at 532.3 eV), respectively. The XPS results confirm the MnO_2 formation, which is consistent with the results of XRD measurement.

The influence of reaction condition on electrochemical activity is also investigated. From Fig. 3(a), the current response of CFC/MnO_2 composites obtained at 3h (10mV/s) is the largest due to the large active surface area, indicating that it could have the highest specific capacitance. This is confirmed by the relationship between the *C* of CFC/MnO_2 composites and hydrothermal time (Fig. 3b). The maximum 2.99 F/cm^2 (291 F·g^{-1}) is obtained for CFC/MnO_2-3h composite. While with further prolonging of reaction time, the loading of MnO_2 on CFC becomes higher, and the MnO_2

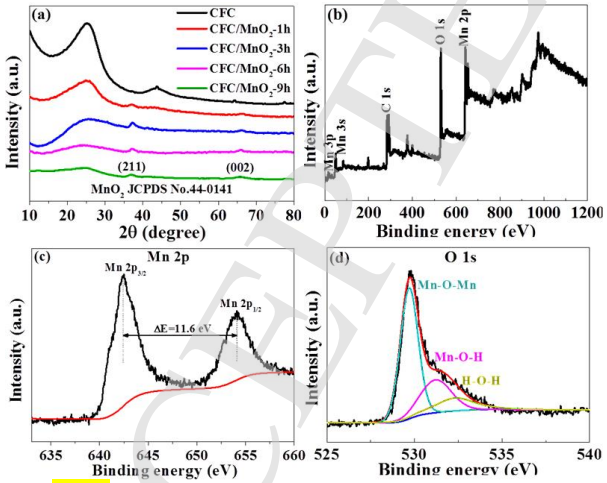

Fig. 2. (a) XRD patterns of pure CFC and CFC/MnO_2 composites obtained at different times. XPS spectra of CFC/MnO_2 composites: (b) full spectrum and detailed spectra of (c) Mn 2p and (d) O 1s.

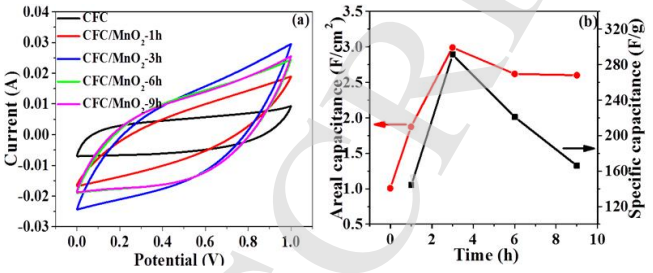

Fig. 3. Electrochemical performances of CFC and CFC/MnO_2 obtained at 140℃ at different times in a 1M Na_2SO_4 aqueous electrolyte: (a) cyclic voltammetric curves (CVs) at a scan rate of 10 mV/s; (b) areal capacitance and gravimetric capacitance of different CFC/MnO_2 composites at 10 mV/s.

NWs evolve into MnO_2 nanorods, limiting the efficient utilization of MnO_2 and reducing the electrochemical properties of composites.

Since the CFC/MnO_2-3h composite exhibits the maximum *C*, it is used as a representative in the following electrochemical analysis. Fig. 4(a) shows the CVs of CFC/MnO_2-3h composite at different scan rates (5-200 mV/s). Although there are no obvious redox peaks, the typical quasi-rectangular shape at low scan rate indicates the apparent pseudocapacitive characteristics of composite due to Faradaic reactions.[22] As the scan rate further increases, the shape of CVs significantly deviates from the rectangle due to some polarizations caused by incomplete adsorption of electrolyte ions on the electrode surface.[23] The GCD curves of CFC/MnO_2-3h composites at different current densities are nearly triangular symmetrically (Fig. 4b), proving excellent pseudocapacitance property of the electrode.[24] The *C* of the active material calculated from the discharge curves is about 3.88 F·cm^{-2} (345 F·g^{-1}) at a discharge current of 5 mA·cm^{-2} (inset in Fig. 4b), which is higher than some reported in previous literatures at the same discharge current density.[4,10,20,25,26] Fig. 4(c) shows the impedance spectra of CFC/MnO_2-3h composite before and after 3000 charge-discharge cycles at a current density of 10 mA·cm^{-2}. The intersection of the semicircular arc and the x-axis, which is defined as equivalent series resistance (R_s), includes the resistances of electrolyte and electrode material itself, and the contact resistance between them. The radius of the semicircular arc represents the transfer resistance (R_{ct}) of the charge during charging-discharging process. The R_{ct} increases significantly after 3000 cycles, which might cause capacitance decrease. The results in Fig. 4(d) show that the specific capacitance (at a current density of 10 mA/cm^2) remains about 91.5 % after 3000 cycles, indicating that the material has good cycle stability.

Furthermore, the CFC/MnO_2-3h composite was used to construct CFC/MnO_2//CFC/AC-ASC. The CVs obtained at

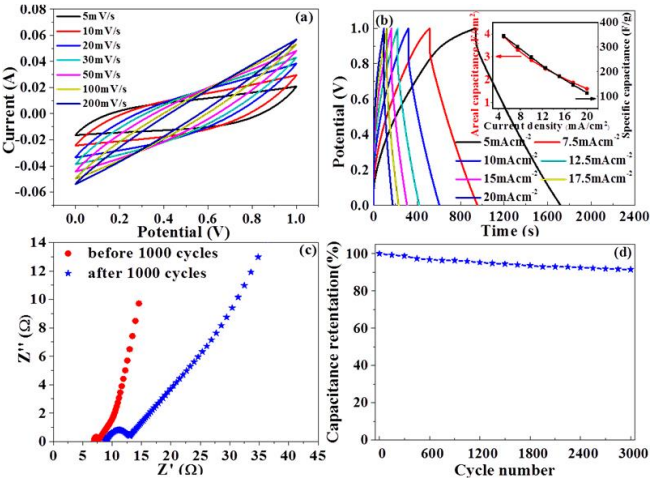

Fig. 4. (a) Cyclic voltammograms of CFC/MnO_2-3h composites at different scan rates in a 1M Na_2SO_4 electrolyte; (b) charge-discharge curves of CFC/MnO_2-3h composites at different current densities, the inset is its areal capacitance and gravimetric capacitance; (c) electrochemical impedance spectra of electrodes at open circuit potential in the frequency range from 0.01 Hz to 100 kHz; (d) cycling performance of CFC/MnO_2-3h composites at a current density of 10mA/cm^2.

different potential windows (scan rate of 100 mV/s) show a stable electrochemical window reaching up to 2 V (Fig. 5a). The CVs at different scan rates present good symmetrical and nearly rectangular shapes even at a high scan rate of 200 mV·s^{-1} (Fig. 5b), indicating good capacitive behavior.[10,27] The good linear profiles of GCD curves in Fig. 5(c) further prove the perfect electrochemical property of the device.[10] The plateau in the GCD curves during the charging process may be related to a higher R_s, as further confirmed by the EIS data (Fig.5 d). The highest C calculated from discharge curves is about 194 mF·cm^{-2} at a discharge current of 2 mA·cm^{-2} (inset in Fig. 5c), showing good capacitance performance. No obvious semicircle in the high frequency region can be seen from the impedance spectrum (Fig.5 d), indicating small transfer resistance during mass transfer process. Fig. 5(e) shows the stability of CFC/MnO_2//CFC/AC-ASC at a current density of 20 mA/cm^2. The capacitance still remains about 88.2 % after 3000 cycles, demonstrating good cycle stability. Fig.5 (g) shows the Ragone plot of CFC/MnO_2//CFC/AC-ASC. The maximum energy density (0.110 mWh/cm^2) and maximum power density (50.0 mW/cm^2) confirm good electrochemical properties.

In summary, MnO_2 nanowires on carbon fiber cloth (CFC/MnO_2) have been successfully synthesized by a facile hydrothermal method and used as an electrode of aqueous asymmetric supercapacitor. It is found that the hydrothermal reaction time affects the morphology and electrochemical performances of MnO_2. The MnO_2 NWs obtained at 3h

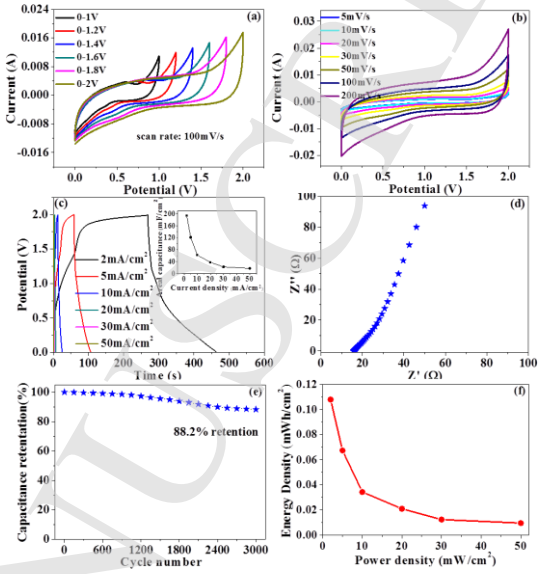

Fig. 5. (a,b) CVs of CFC/MnO_2//CFC/AC-ASC at different potential windows and different scan rates, respectively. (c) Charge/discharge curves of the CFC/MnO_2//CFC/AC-ASC at different current densities, the inset is its areal capacitance. (d) EIS spectrum of CFC/MnO_2//CFC/AC-ASC. (e) Cycling performance of CFC/MnO_2//CFC/AC-ASC at 20 mA/cm^2. (f) Ragone plot of the CFC/MnO_2//CFC/AC-ASC.

exhibit excellent supercapacitor performance with a high specific capacitance of 3.88 F·cm^{-2} at a current density of 5 mA·cm^{-2} and a cycling retention of 91.5 % after 3000 repeated measurement. Furthermore, the CFC/MnO_2//CFC/AC-ASC shows outstanding electrochemical performance such as high specific capacitance of 194 mF·cm^{-2} at a charge-discharge current density of 2 mA·cm^{-2} and high energy density of 0.108 mWh·cm^{-2} at power density of 2 mW·cm^{-2}, exhibiting great promise for large-scale supercapacitor applications.

Acknowledgement

This work was supported by the National Natural Science Foundation of China (Nos. 51572242, 11372280 and 11472191), the Zhejiang Provincial Natural Science Foundation of China (No. LY16E020011), the 521 Talent Project of Zhejiang Sci-Tech University, the Program for Innovative Research Team of Zhejiang Sci-Tech University (No. 15010039-Y) and the Opening Fund of State Key Laboratory of Structural Analysis for Industrial Equipment of Dalian University of Technology (No. GZ1704).

References

1. C. Guan *et al.*, *Energy Environ. Sci.* **4**, 4496 (2011).
2. Z. Su *et al.*, *Energy Environ. Sci.* **7**, 2652 (2014).
3. Y. Qiu *et al.*, *J. Appl. Phys.* **123**, 084103 (2018).
4. D. Guo *et al.*, *J. Mater. Chem. A* **2**, 8833 (2014).

5. Y. Li *et al*., *Langmuir* **29**, 493 (2013).
6. B.E. Conway *et al*., *J. Power Sources*. **66**, 1 (1997).
7. S.W. Lee *et al*., *ACS Nano* **4**, 3889 (2010).
8. Q. Li *et al*., *Nano Lett*. **12**, 3803 (2012).
9. M. Toupin *et al*., *Chem. Mater*. **16**, 3184 (2004).
10. J.Y. Tao *et al*., *Nanoscale*. **6**, 2922 (2014).
11. X.H Wang *et al*., *Biosens. Bioelectron.* **105**, 22 (2018).
12. J.J. Chen *et al*., *Appl. Sur. Sci.* **360**, 534 (2016).
13. N. Jabeen *et al*., *Adv. Mater*. **29**, 1700804 (2017).
14. N. Jabeen *et al*., *ACS Appl. Mater. Interfaces* **8**, 33732 (2016).
15. H. Xia *et al*., *Funct. Mater.s Lett.* **2**, 13 (2009).
16. S.C. Sekhar *et al*., *Nano Energy* **36**, 58 (2017).
17. S. Devaraj *et al*., *J. Phys. Chem. C* **112**, 4406 (2008).
18. Z.S. Wu *et al*., *ACS Nano* **4**, 5835 (2010).
19. M. Tamaddoni Saray *et al*., *Electrochim. Acta*. **222**, 505 (2016).
20. K.B. Xu *et al*., *J. Mater. Chem. A* **2**, 4795 (2014).
21. L.H. Bao *et al*., *Nano Lett*. **11**, 1215 (2011).
22. M. Huang *et al*., *J. Power Sources*. **252**, 98 (2014).
23. Y.C. Tsai *et al*., *Materials.* **9**, 246 (2016).
24. A. G. Mohammad *et al*., *J. Mater. Chem. A* **5**, 3547 (2017).
25. F.Z. Deng *et al*., *Electrochim. Acta*. **176**, 359 (2015).
26. H. Jiang *et al*., *J. Mater. Chem*. **22**, 16939 (2012).
27. Y.Y. Sun *et al*., *Electrochim. Acta*. **178**, 823 (2015).